RESEARCH ARTICLE



Investigating the Compositional Space of Gas-Phase Synthesized Fayalitic Model Slags Aiming at Cobalt Recovery

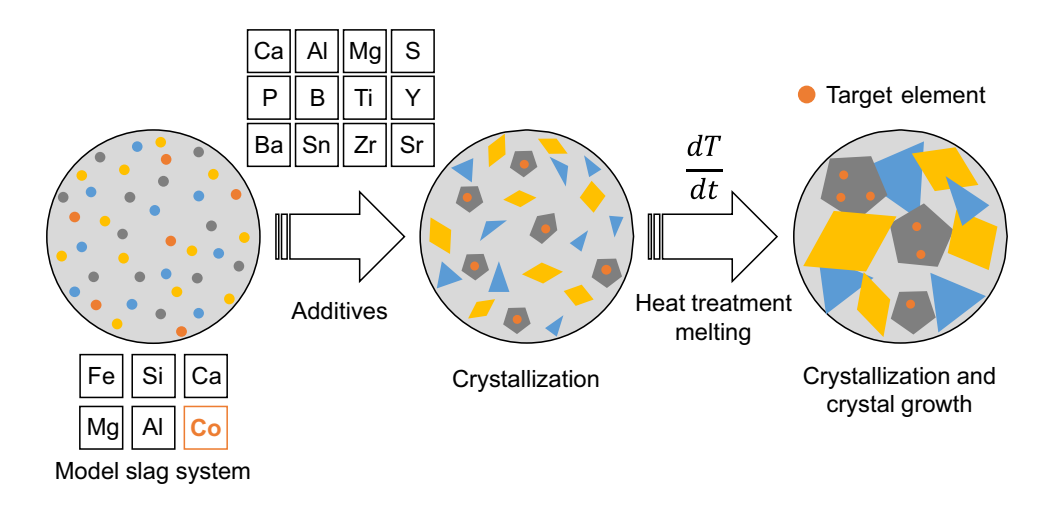
Manuel Vollbrecht 10 · Krishnanjan Pramanik 1,30 · Lucio Colombi Ciacchi 1,30 · Lutz Mädler 1,20

Received: 7 March 2024 / Accepted: 6 July 2024 / Published online: 25 July 2024 © The Author(s) 2024

Abstract

Metallurgical waste streams contain minor yet significant contents of valuable and scarce elements which are commonly lost due to their low concentrations. The necessity of developing efficient recycling methods of these chemically diverse material systems is constantly gaining both public and technological attention since resource demands of high-technology elements are expected to rise drastically in the future. A novel approach to recover diluted elements from slags is the concept of Engineered Artificial Minerals (EnAM) which aims at entrapping target elements in separable crystalline phases. In this study, slag synthesis through flame spray pyrolysis (FSP) and characterization experiments are combined with theoretical density functional theory (DFT) calculations to identify potential EnAM for Co recovery. Upon validating the viability of stoichiometric slag synthesis and the DFT framework, it is shown that the actual occurrence of flame-synthesized phases can be predicted considering their computed enthalpy of formation. The thus-defined compositional space, which is spanned by potentially forming slag compounds, is employed to identify promising additives for EnAM formation. Systematic analysis of the additive effect on crystallization revealed that Co crystallizes in a Fe–Mg-Co–O cubic spinel, making this phase a good EnAM candidate.

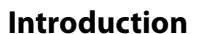
Graphical Abstract



Keywords Engineered artificial minerals · Slag crystallization · Fayalitic slag · Recycling

The contributing editor for this article was Alexandros Charitos.

Extended author information available on the last page of the article



It has been projected that the demand for cobalt will increase by up to 1500% to realize carbon neutral technologies in the European Union by 2050 [1]. Keeping its importance for the



green energy future in mind, cobalt has been classified as a critical raw material due to its inhomogeneous geological occurrence. The development of robust and efficient recycling technologies up to the establishment of circular value chains for critical raw materials, especially for high-technology elements such as cobalt, is of great socio-ecological interest and marks an important step towards sustainable resource handling [2].

Metallurgical slags are a known secondary source for valuable elements and have been gaining significant attention regarding recyclability [3–7]. Copper slags, often referred to as fayalitic slags, are a Fe-rich metallurgical waste generated as a by-product during smelting, converting and refining of copper ore. Along with conventionally applied fluxes in metallurgical processes, their predominating chemistry is comprised of the system FeO-SiO₂-CaO-MgO-Al₂O₃. However, the composition of copper slags is much more diverse depending on various factors such as the ore used, the processing history of the slag and added slag modifiers to favorably tune its properties. For example, basic oxides such as CaO and MgO are added to control the melting temperatures [8] and the viscosity of the molten slag [9]. Hence, a vast number of additional elements may be found in copper slags such as Ni, Zn, Mn, Ti, S, Na, K, Pb, Sn, and Cr as well as minor contents of valuable Mo, Co, and residual Cu from the metallurgical extraction. Considering Co, its content reportedly varies from as low as 0.043 wt% [10] to as much as 4.09 wt% [7].

Current slag recycling techniques comprise flotation methods as well as multi-stage pyrometallurgical and hydrometallurgical approaches [5]. However, hydrometallurgical methods consume significant amounts of hazardous chemicals such as acidic agents, thus, posing challenges to waste handling [11]. Similarly, pyrometallurgical processes are prone to the release of hazardous by-products such as off-gases and volatile metal compounds [12]. Further challenges associated with pyrometallurgical processing stem from metals with high oxygen affinity (e.g., Li) which migrate to the slag inhibiting their efficient recovery [13]. It has been suggested that recovery of valuable elements from slags can be achieved by modifying and controlling the slag mineralogy. In that scope, the slag composition, its thermal history, and atmosphere during processing need to be controlled to engineer the microstructure of a slag system [14]. The recovery approach foresees the enrichment of a target element in a crystalline phase through favorably tuning the slag composition and controlling the thermal slag processing. This target crystalline phase differs in composition and properties from the surrounding slag matrix comprised of other phases which can be either crystalline or amorphous. A crystalline phase rich in a valuable target element, i.e., Co, is referred to as engineered artificial mineral (EnAM) and can originate from (near) equilibrium and out-of-equilibrium slag processing conditions, i.e., during slag cooling. Slow cooling is associated with the formation of thermodynamically stable

phases near the system's equilibrium. Rapid cooling may restrict the crystallization kinetics of the slag system favoring the formation of meta-stable crystalline phases. Recovery of the target elements as a secondary raw material becomes feasible after separating the EnAM from the slag matrix with established methods such as crushing and grinding followed by flotation. Recent studies focused on the recovery of Li from the Li₂O-MgO-Al₂O₃-SiO₂-CaO-MnO slag system using the EnAM processing route. It was found that Li forms crystalline aluminates and manganates making both the Li-Al-O and Li-Mn-O systems promising EnAM candidates [15]. In fact, the EnAM potential of the LiAlO₂ phase was demonstrated in flotation experiments with high recovery rates [16]. Further EnAM identification was conducted in the favalitic Fe-Si-Al-Ca-O slag system arising from pyrometallurgical treatment of waste from electrical and electronic equipment (WEEE) for the recovery of Ta. Here, Ta could be enriched in various ternary and quaternary perovskite structures containing Fe, Si, and Ca [17].

However, the crystalline phases that form in the slag having the target element Co as a crystal component, i.e., an EnAM, are yet unknown. Due to the elemental complexity of the metallurgical system, a vast number of crystalline phases may form within the slag. The space spanned by all possible crystalline phases, both stable and meta-stable, including the unknown EnAMs make up the *compositional space* of the slag system. It is hypothesized that incorporating additives in the slag triggers formation of EnAMs rich in the target element through winning the thermodynamic battle over other competing phases. This approach requires a comprehensive understanding of the crystallization pattern in a given slag and the influence of additives.

The present study aims at investigating the crystallization and the influence of additives in model favalitic slags synthesized via flame spray pyrolysis (FSP). The experimental analyses are guided by predictions from ab initio thermodynamics computed using the framework of density functional theory (DFT) with the goal of identifying promising additives for EnAM formation to recover Co. FSP is a highly efficient method to synthesize multicomponent metal oxides with homogeneously distributed elements on the length scale of few nanometers. It is further capable to produce binary and multicomponent metal oxides such as spinels and perovskites [18]. Consequently, slag synthesis with FSP represents a generic approach to obtain varying model compositions with freely selectable additives mimicking real-world slag systems and, thus, allowing for the exploration of the slag's compositional space. It is further possible to computationally determine the formation enthalpies of a large number of relevant phases using DFT and to obtain a detailed picture which phases are most likely to form within the compositional space enabling the identification of phases that can be exploited as potential EnAMs.



Methods

The presented work for the identification of EnAM phases combines theoretical investigations comprising database screening and density functional theory calculations with experimental material analytics of model slags synthesized with flame spray pyrolysis. A schematic representation of the research process is provided in Fig. 1 in the Supplementary Material as guidance for the applied methodology.

Database Screening

In the context of this study, the compositional space is defined with all the possible stable crystalline phases made of the major elements of the slag, and any other possible element that can be incorporated as additive that promotes EnAM formation. The search for such crystals was conducted in the Inorganic Crystal Structure Database (ICSD) [19]. An initial screening for Co-containing phases resulted 1044 entries for ternary oxides and 2752 entries. This vast number of experimentally reported phases was narrowed down for potential EnAM candidates by taking the following aspects into account. All crystalline phases containing (i) hazardous (e.g., Ni, Pb) or (ii) radioactive (e.g., U) elements were excluded from further consideration to ensure work safety and slag synthesizability. Further, (iii) crystals with highly expensive (e.g., Au, Ir) or (iv) scarce elements (e.g., Ce, Nd) as well as phases containing elements with (vi) liquid (Br, Hg) or gaseous (e.g., F, Cl) aggregate state at ambient conditions are considered irrelevant for this study because they cannot be handled easily as slag additives. The maximum number of external elements in the crystals was also restricted to two during the database search to avoid further complexity. This initial screening provided a pool of potential additives and associated Co-containing crystalline oxide phases, as shown schematically in Fig. 1, with (1) one or more elements from the slag components and (2) one external element that can be added to the slag. In addition to Co-containing crystals, other possible crystalline phases without Co, i.e., the ternary, quaternary oxides of the slag constituents, were also included in the pool. In order to identify potential EnAM candidates, it is crucial to understand which crystals from the pool are more likely to form in the multicomponent model slag.

Density Functional Theory (DFT) Calculations

As a useful indicator of the driving force for the formation of EnAM phases, their enthalpy of formation (ΔH_f) computed at the level of DFT is considered [20, 21]. With respect to other empirical approaches at base of thermochemical

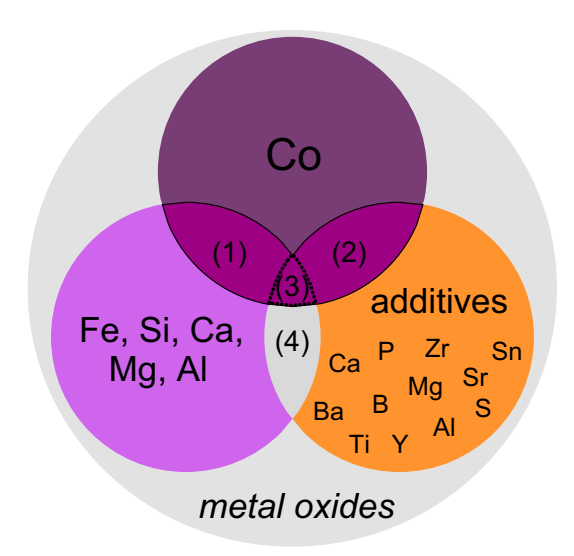


Fig. 1 Approach of ICSD database screening for crystalline Cocontaining oxide phases: (1) crystalline phases containing Co and slag constituents, (2) crystalline phases containing Co and additives, (3) crystalline phases containing Co as well as slag constituents and additives, (4) crystalline phases containing slag constituents and additives. Regions (1), (2), and (3) comprise the targeted EnAM used for Co recovery

databases, this approach is able to capture subtle electronic-structure effects such as magnetic ordering or Jahn–Teller distortions that may dictate the stability of transition-metal oxides. For this study, the calculations were conducted using the open-source code Quantum ESPRESSO (QE) [22, 23]. The pseudopotentials were taken from the SSSP PBEsol Precision v1.2.0 library [24, 25]. The energy cutoffs were chosen as prescribed in the aforementioned library, e.g., 90 Ry for all the Co-containing phases. Electronic self-interaction error, especially for transition metals, is a well-known issue in DFT, which is addressed with Hubbard-like corrections referred as DFT+U [26]. The 'U' parameter, wherever necessary, was calculated using the self-consistent (first-principles) route as implemented in the QE package [27–29].

The known ground state magnetic ordering was incorporated in the initial structures of phases. Two issues have been pointed out frequently in the literature related to the calculation of the ΔH_f from the corresponding elemental phases. Firstly, the 'U' correction is only applied for the oxide phases, e.g., CoO, and not for elemental metal phases. Secondly, the over estimation of the binding energy of O_2 molecules by DFT has to be corrected for [30]. Both of these issues are known to produce systematic errors in the calculation of ΔH_f . To address these inadequacies, corrections were implemented in the calculations, as prescribed by Jain et al. [31] and Wang et al. [32].



Flame Spray Pyrolysis (FSP)

Conventionally, flame spray pyrolysis is used to synthesize highly crystalline functional nanoparticles [18, 33]. In this study, the FSP route is adapted to synthesize model slag samples in the form of metal oxide nanoparticles allowing for a freely engineerable chemical composition of the slag systems. Due to steep temperature gradients and associated high cooling rates in FSP [34], the potential formation of

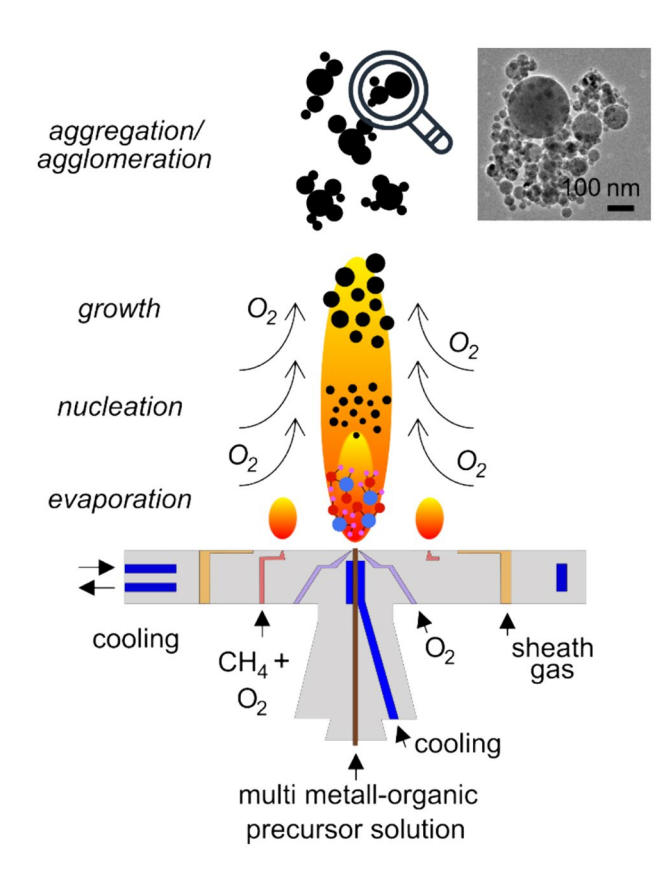


Fig. 2 Schematic reactor set-up of the flame spray pyrolysis including the particle synthesis route in the gas phase. Upon dispersion of the liquid precursor, nanoparticles nucleate, grow, and agglomerate (physically bind to each other) or aggregate (chemically bind to each other) in the gas phase

amorphous, meta-stable, and stable crystalline phases within the slag systems can be assessed. A schematic of the FSP reactor according to Mädler et al. [35] and the nanoparticle formation process is shown in Fig. 2.

During FSP slag synthesis, a liquid precursor solution was fed through a capillary at a constant feed rate (5 mL/min) and dispersed under a pressure drop of 1.5 bar with oxygen gas (Westfalen, purity 5.0) using a Tethis nozzle [35]. The spray was combusted in a self-sustaining flame which was stabilized by a surrounding pilot flame fed with constant gas low rates of 1.5 L/min and 3.2 L/min of methane (Westfalen, purity 3.5) and oxygen (Westfalen, purity 5.0), respectively. Nanoparticles were separated downstream from the gas phase and collected using a glass fiber filter (Whatman, GD/F, Ø 257 mm). The nanoparticle filter cake was removed and sieved (125 µm) to separate remaining filter fibers from the nanoparticle agglomerates.

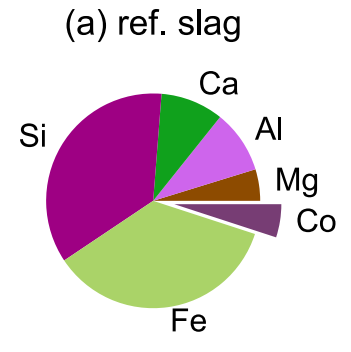
For a precise control of the elemental contents in the slag samples, single metal-organic precursors (cf. Table 1) were first prepared at a metal ion concentration of 0.5 mol/L for each slag element using xylene (VWR) as organic solvent. Subsequently, a multi-metal organic precursor was mixed using high precision pipetes (Eppendorf research® plus 0.5-5 mL, 0.01% inaccuracy at 5 mL setting) to obtain nominal element ratios in the model slag samples as shown in Fig. 3. A total precursor volume of 100 mL was chosen for the slag samples to ensure a maximum particle yield during synthesis. Since single element precursors were prepared at the same molar concentration and a total precursor volume of 100 mL was used in the FSP for the nanoparticle slag synthesis, the elemental atomic fractions depicted in Fig. 3 are equivalent to the individual elemental precursor volumes in the respective liquid precursor solutions.

The experimental methodology is based on a preengineered fayalitic model slag system which arises from a profound literature review [3–7]. It represents a compositional average of reported real slag systems which vary in their geo-position, processing history, and feedstock material. Hence, the chemical slag diversity was broken down to a constant concentration ratio of five

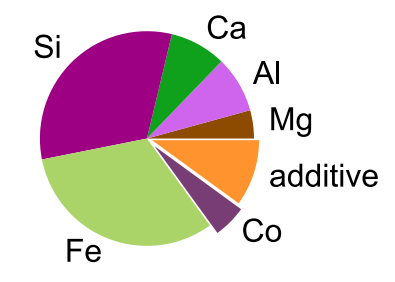
Table 1 Specifications of metal organics used to prepare precursors of 0.5 M concentration for FSP synthesis

Element	Precursor	Provider	LOT number	Concentra- tion (mol/L)
Fe	Ferrocene	Sigma Aldrich	STBK8528	0.5
Si	Tetraethylorthosilicate	Sigma Aldrich	BCBM1319V	0.5
Al	Al-tri-sec-butoxide	Sigma Aldrich	MKCD3129	0.5
Ca	Ca naphthenate	Strem Chemicals	L00182105	0.5
Mg	Mg naphthenate	Strem Chemicals	20981200	0.5
Co	Co naphthenate	Strem Chemicals	L01982107	0.5
P	Triethylphosphate	Sigma Aldrich	MKBQ0206V	0.5
Ti	Ti(IV) isopropoxide	Sigma Aldrich	BCCB4674	0.5

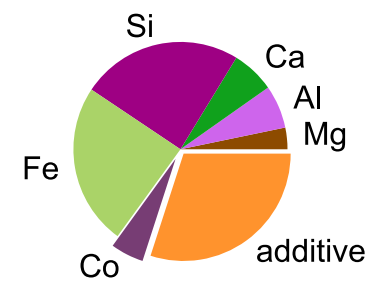




(b) 10 at% additive



(c) 30 at% additive



(d) reduced Si

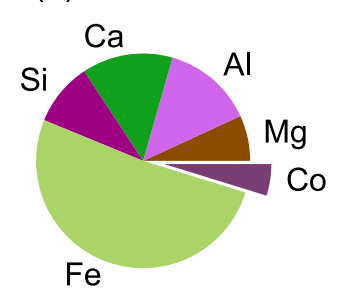
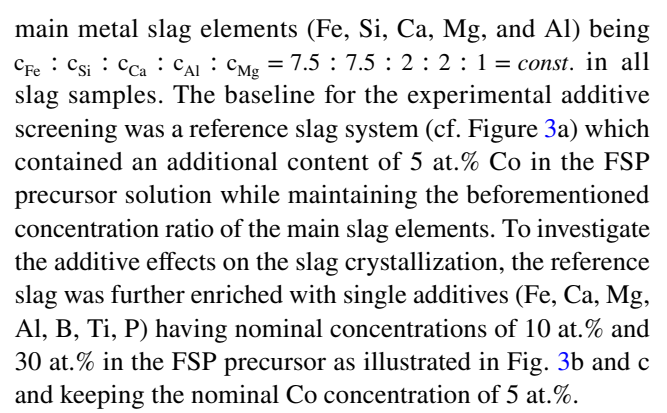


Fig. 3 Nominal ratios of slag metal ions in precursor solution for FSP slag synthesis: **a** model slag system, **b** reference slag system containing 5 at.% Co, **c** model slag system including 5 at.% Co and 10 at.% of additive, **d** model slag system containing 5 at.% Co and 30 at.% of additive



The choice of the additives was based on the analysis of the DFT calculations. To investigate the crystallization of isomorphous phases during FSP, a fourth slag system (cf. Figure 3d) was sprayed which possessed a lowered nominal Si content of 10 at.%, 5 at.% of Co and the same elemental ratio of the remaining base slag elements.

Single-phase nanoparticles (CoFe₂O₄, CoAl₂O₄, MgCo₂O₄, MgFe₂O₄, MgAl₂O₄, FeAl₂O₄) were synthesized with a respective stoichiometric metalorganic precursor solution of 60 mL and used to validate the combined approach with the previously described theoretical DFT framework.

X-Ray Diffraction (XRD)

A Bruker Discover D8 diffractometer in Bragg–Brentano geometry equipped with a monochromatic Cu- K_{α} radiation source ($\lambda = 1.5406$ Å) and a Bruker LynxEye XE-T linear detector (192 channels) was used to analyze the crystallographic structure of the slag nanoparticles. All samples were measured from 5° to $100^{\circ}~2\theta$ diffraction angle with an angle increment of 0.051° , an integration time of 7.5 s per angle increment, and a beam-opening angle of 0.26° . All samples were deposited on a single-crystal silicon wafer to ensure a minimal signal of the substrate. The analyses and Rietveld refinements were carried out using the Software BRASS (Version 2.4.0). Crystallographic structure models were collected from the Inorganic Crystal Structure Database (ICSD).

Scanning Electron Microscopy with Energy Dispersive X-Ray Spectroscopy (SEM/EDX)

Bulk chemical compositions of the as-sprayed slag particles were obtained from EDX measurements. Particles were deposited on a carbon sticker and sputtered with gold to increase electrical conductivity of the metal oxide nanoparticles. The measurements were performed with a Zeiss SUPRA® 40 SEM system equipped with a Bruker XFlash® 6–30 detector under high vacuum (residual pressure of 10^{-5} mbar) and suitable magnifications.



Scanning Transmission Electron Microscopy (STEM)

A Thermo Fisher Spectra 30/300 probe-corrected STEM (Thermo Fisher Scientific Inc., USA) equipped with a SuperX EDX detector and a high-angle annular dark field (HAADF) detector operated at 300 kV was employed to characterize the spatial elemental distribution at the nanoscale and examine the nano-crystallinity in the slag samples. EDX data were analyzed and visualized with the Thermo Fisher Velox software. Fourier filtering for determining the crystal lattice distances was performed with the open-source software ImageJ. For the measurements, the as-prepared nanoparticles were dispersed in pure ethanol (Sigma Aldrich, purity≥99.5%) followed by ultrasonification of 3 min to break up physical bonding between single nanoparticle aggregates. Two drops of liquid were deposited onto an amorphous carbon Ni grid and dried.

Results and Discussion

Validation of Stoichiometric Slag Synthesis and DFT Framework

In order to investigate the compositional effect on the crystallization of the slag system, a precise and engineerable slag chemistry has to be ensured. It is a well-known challenge in gas-phase synthesis that very volatile elements may be lost in the gas phase rather than taking part in the particle formation process. The phenomena applies, for example, to sulfur which tends to form gaseous SO_x as a reaction product in the conventionally oxygen-rich flame environment [33] due to its low electronegativity compared to oxygen [36]. Hence,

the need to validate the compositional engineerability of multi-elemental oxides produced in the FSP process arises.

The left graph in Fig. 4 compares the measured elemental concentrations of the slag nanoparticles with the nominal concentrations shown in Fig. 3. The visualized precursor calculations only take the non-oxygen elements into account since O₂ is added to the slag composition through the oxidation reactions in the gas phase. Therefore, the oxygen content is subtracted from the actual compositions and the elemental fractions are renormalized to allow for a comparison with the liquid precursor stoichiometry. The as-measured compositions are provided in the Supplementary Material. Data points having an error bar represent an average of obtained atomic concentrations across multiple samples (cf. Figure 2) with the same respective elemental content. The error bar is the " 1σ " standard deviation. The comparison of measured and expected concentrations reveals that a stoichiometric nanoparticle synthesis is feasible with up to seven different precursor elements in a single-flame spray process. The elemental diversity comprises earth alkali metals (Mg, Ca), transition metals (Co, Fe, Ti), metals (Al), as well as nonmetallic elements (P). Further, the engineerability of element contents ranges from concentrations as low as 3 at.% to roughly 55 at.%. Despite different mixtures of single metal precursors with varying concentrations, precise reproducibility of the slag composition through FSP synthesis is ensured as the statistical deviation of the elemental contents is negligibly small. The composition analysis of single nanoparticle aggregates through EDX in STEM measurements (Fig. 3 right) confirmed the results of the bulk EDX in SEM measurements. Aggregate compositions are in good agreement with the expected values which implicates a homogeneous elemental distribution across the nanoparticles. It

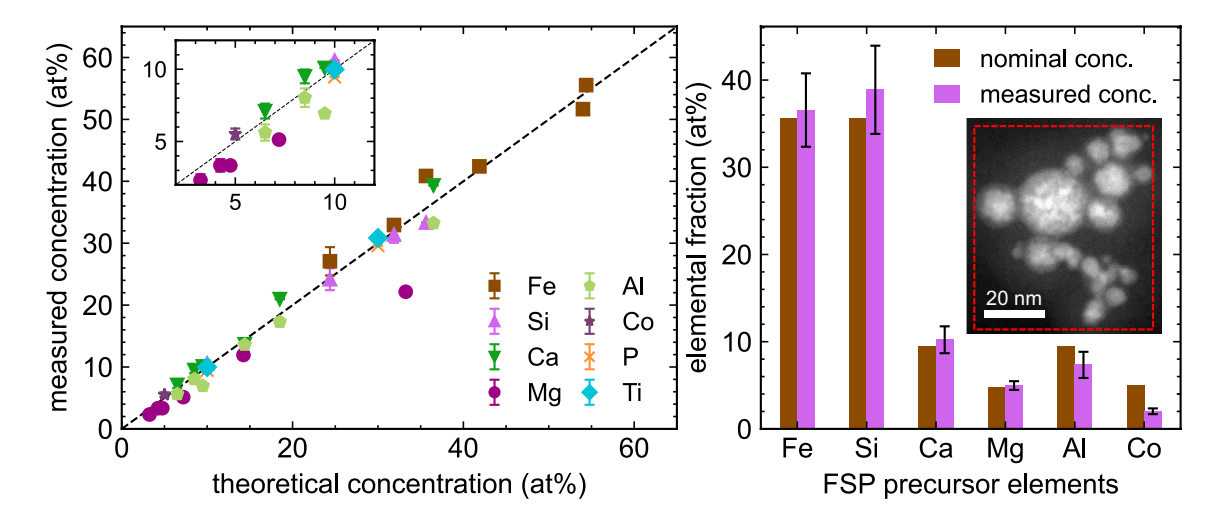


Fig. 4 Chemical compositions of flame-sprayed slag samples measured with EDX: bulk measurements in SEM (left) and representative nanoscale measurement for reference slag in TEM compared with desired composition (right)



further allows for representative analyses by considering only single aggregates (cf. STEM insert in Fig. 3).

Homogeneous, solid nanoparticles as shown in Fig. 4 are produced by gas-phase nucleation, growth through sintering and coalescence and final aggregation which is referred to as the gas-to-particle route. Suitable precursor solutions exhibit generally low boiling temperatures, high vapor pressures (high volatilities) and high combustion enthalpy densities resulting in high flame temperatures. [18, 37]

The precursors used in this study possess similar boiling points and vapor pressures; thus, they maintain these favorable physiochemical properties in the FSP precursor mixtures (cf. Table 2). Xylene as the solvent of choice provides a self-sustaining high temperature flame, having a combustion enthalpy of -4550 kJ/mol [38]. Further, it was stated in the literature that volatile carboxylates (R–COO⁻) in the precursor solution or in the spray droplets favor the gas-to-particle conversion [39]. In the present study, naphthenates in mineral spirits are used as precursors bearing the favorable deprotonated carboxy group.

Besides suitable precursor properties, it has been proposed that the driving mechanism for the formation of homogeneous nanoparticles in a spray flame is the occurrence of micro-explosions of the precursor droplets with instantaneous release of metal ions and mass transfer to the gas phase [40]. One main requirement is the possibility of precursor decomposition over a wide temperature range, which is ensured by low precursor boiling points [41]. Measurements of temperature profiles in the FSP process revealed residual temperatures above 600 K at 20 cm above the dispersion nozzle, which still exceeds the boiling points of the used precursors [34]. Therefore, it is assumed that process conditions during slag synthesis favored droplet disruptions and, thus, the observed chemical homogeneity, as investigated elsewhere [42–44].

Overall, the measurements exhibit fluctuations in single concentrations well below 5 at.%. Consequently, model slags

with reproducible composition can be obtained through the FSP process with suitable precursor-solvent mixtures.

Experimental values of formation enthalpies ΔH_f are readily available for binary oxides [45]. In order to validate the computational method employed in this study, the computed values of ΔH_f of binary oxides are reported in Fig. 5. The phases of interest are the binary oxides of the model slag metals, namely Al₂O₃, MgO, SiO₂, CaO, FeO, Fe₂O₃, Fe₃O₄, CoO, and Co₃O₄. Without the corrections mentioned in the previous section, the values of ΔH_f deviate from the experimental reports significantly. It is also noticeable that the deviations are more profound for the oxides of Fe and Co (the top five) compared to the oxides of Al, Mg, Si, and Ca. This can be attributed to the self-interaction errors in standard DFT for transition-metal oxides, as discussed earlier. However, when the proper corrections were incorporated, the values become in very good agreement with the

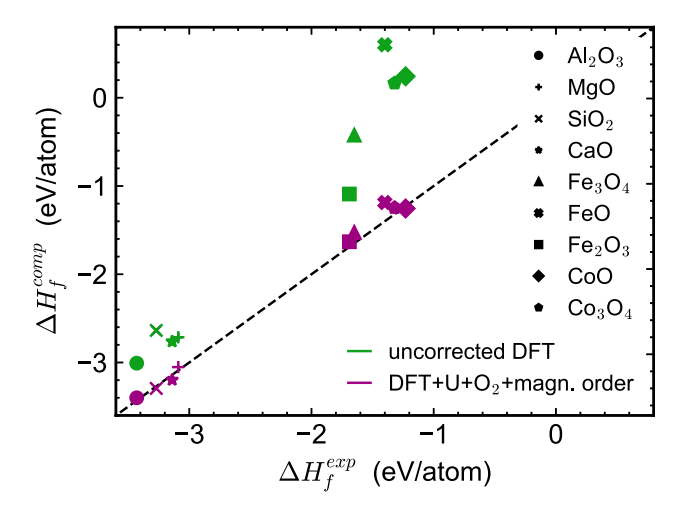


Fig. 5 Comparison of experimentally reported formation enthalpies ΔH_f^{exp} from [45] with computed formation enthalpies ΔH_f^{comp} of the slag binary oxide components

Table 2 Physical properties of metal–organic precursors (data retrieved from corresponding safety data sheets)

Precursor	Flame point (°C)	Boiling point (°C)	Vapor pressure	Melting point
Ferrocene	No data	249	<0.1 hPa (40 °C)	172 °C
Tetraethylorthosilicate	45	168	<1 hPa (20 °C)	− 82.5 °C
Al-tri-sec-butoxide	26	200-206	23 hPa (195 °C)	No data
Ca naphthenate*	79*	214-216*	0.22 hPa (20 °C)*	- 10 °C (1 bar)*
Mg naphthenate*	79*	214-216*	0.22 hPa (20 °C)*	- 10 °C (1 bar)*
Co naphthenate*	79*	214-216*	0.22 hPa (20 °C)*	- 10 °C (1 bar)*
Triethylphosphate	130C	215	0.51 hPa (25 °C)	− 56.4 °C
Ti(IV) isopropoxide	41	232	133 hPa (63 °C)	14–17 °C
Xylene (solvent)	25	136–140	5–10 hPa (20 °C)	− 34 °C

Naphthenates are provided as mixtures of carboxylic acids with mineral spirits. Therefore, physical properties are unavailable. In replacement for the scope of the discussion, physical properties of 1-dodecene (constituent in diesel fuel) are provided for the marked (*) precursors



experiments. These corrections were, therefore, applied to all the ternary and quaternary oxides considered further in this study.

Prediction of Crystalline Phases from FSP Through DFT Calculations

The values of ΔH_f computed with DFT represent the thermodynamic driving forces to form the respective oxide phases at 0 K. Predicting the free energies of formation at high temperature is possible but computationally much more demanding, because expensive calculations of the phonon dispersion are required to quantify the entropic contributions. However, simple and quick estimates of ΔH_f do already provide a first indication whether a mixed oxide phase may be more stable than the parent binary compounds, and may, thus, be able to form in FSP experiments. Figure 6 reports the computed ΔH_f of six-mixed spinel phases containing Co, Fe, Mg, and Al together with their parent compounds plotted against the at.% of the elements. Stable phases should lie below the linear combination of the energies of the separated parent compounds, forming a convex hull [46, 47]. The calculations predict that CoFe₂O₄ and FeAl₂O₄ are stable, MgCo₂O₄

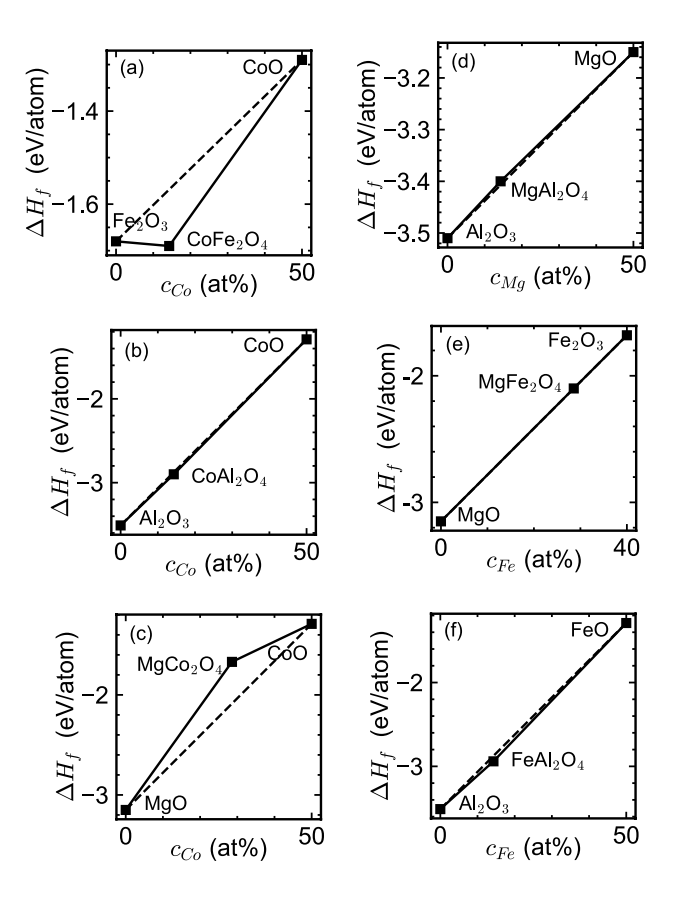


Fig. 6 Stability assessment considering the ΔH_f of isomorphous spinel phases and their parent binary oxides

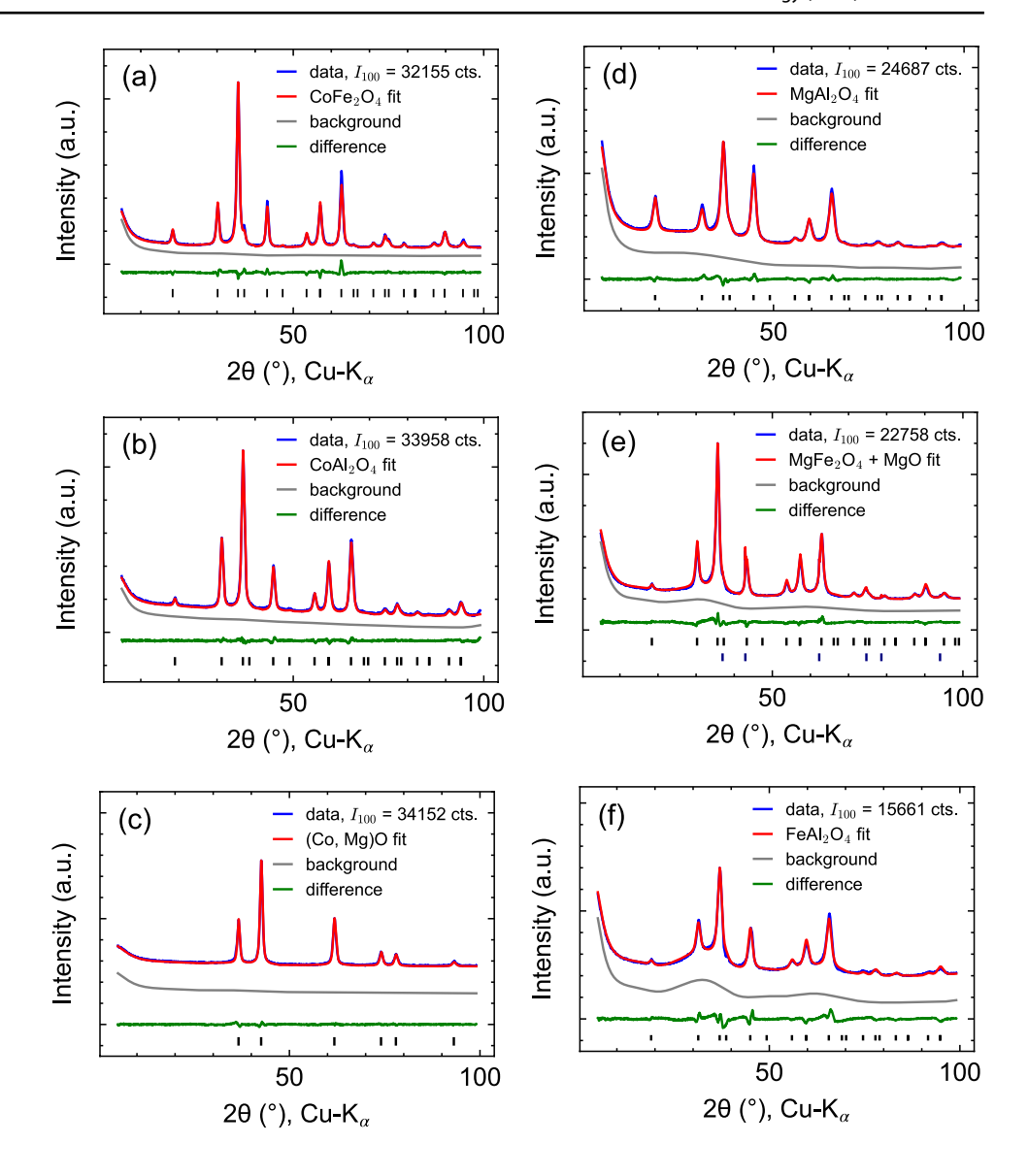
is unstable, whereas $CoAl_2O_4$, $MgFe_2O_4$, and $MgAl_2O_4$ are either slightly favored or as stable as a combination of the parent compounds. Due to the approximate character of the computational predictions, it shall be noted that differences smaller than about 0.05 eV/atom are insignificant [47–50]. In particular, it needs to be verified with care if the predicted stable phases form in the kinetically-driven FSP process with high cooling rates in the order of 10^6 – 10^7 Ks⁻¹ as estimated from experimentally determined gas velocities reaching up to 200 ms⁻¹ and temperature gradients of 200–300 Kcm⁻¹ [34].

In order to validate the formation of the predicted spinel phases, precursors of the metal elements at their respective stoichiometry were mixed and employed in the FSP process. Figure 7 shows the X-ray diffraction patterns of the pure phase samples. Formation of pure cubic Fd3m (a) $CoFe_2O_4$ (crystallite size (16.6 ± 1) nm) and (f) $FeAl_2O_4$ (crystallite size (7.4 ± 0.1) nm) spinel phases nicely confirmed the theoretical prediction. The experiments also showed the preferential formation of (b) CoAl₂O₄ (crystallite size (12.8 \pm 0.7) nm) and (d) MgAl₂O₄ (crystallite size (9.5 ± 0.4) nm). In case of (d) Mg-Fe-O, additional intensity peaks indicate the presence of the crystalline cubic MgO phase along with the MgFe₂O₄ compound (crystallite size (6.2 ± 0.1) nm), in line with the calculation of a zero enthalpy of reaction (Fig. 6e). In case of Mg-Co-O, where MgCo₂O₄ is predicted to be unstable, the peaks observed in XRD in fact reveal the formation of a crystalline cubic Fm3m solid solution of (Co, Mg)O rather than the spinel. The Rietveld refinement (Fig. 7c) resulted in a calculated lattice parameter $a_{\text{exp}} = 4.243 \text{ Å}$ which is in accordance with the expected value of $a_{\text{theo}} = 4.248 \text{ Å}$ obtained from Vegard's law assuming that CoO (ICSD collection Code 9865) and MgO (ISCD collection code 9863) form a solid solution with the molar ratio c_{Co} : $c_{Mg} = 2:1$. Considering the ionic radii of Mg²⁺ and Co²⁺ in the sixfold coordination in their pure isomorphous oxides, Goldschmidt's rule for the formation of solid solution by ion substitution holds [51]. However, to form a spinel phase with Mg, the Co ion would need to be in an oxidation state higher than its preferred + 2 state (cf. Supplementary Material). In general, MgO is a very common phase in FSP synthesis because, unlike other earth alkali metals (e.g., Sr), Mg tends not to react with the residual carbon in the flame to form a carbonate [39].

These combined results (Figs. 6 and 7) show that DFT calculations of ΔH_f are good indicators for the actual formation of a specific phase in the FSP process, at least for reaction enthalpies lower than about -0.1 eV per atom. All of these phases, in particular the spinels, have been produced in FSP with different precursors and process parameters [39, 52–55], making the stability prediction largely independent of the precursor systems and the precise process conditions.



Fig. 7 XRD patterns and Rietveld refinements revealing expected structural crystallinity of as-sprayed single phases as predicted by DFT calculations: a CoFe₂O₄ (ICSD collection code 29630), b CoAl₂O₄ (ICSD collection code 78402), c (Co, Mg)O (ISCD collection code 9865), d MgAl₂O₄ (ICSD collection code 13861), e MgFe₂O₄ (ICSD collection code 24767), and MgO (ICSD collection code 9863), f FeAl₂O₄ (ICSD collection code 9863)



Definition of Compositional Space and Additive Screening

In the context of this study, the compositional space consists of all possible oxides (crystalline phases) of all the elements that belong to the slag system and the potential additives which may contribute to the crystallization of a Co-containing EnAM. The search for potential EnAM in such vast compositional space was narrowed down by the initial screening method described earlier. The considered crystalline phases are classified as the binary oxides, spinels, olivines, pyroxenes, perovskites, and all other phases grouped as "other." As shown in Fig. 8, they are mapped with respect to their ΔH_f as a function of Co at.%. Among the binary oxides, CaO, SiO₂, Al₂O₃, and MgO reside around the energetic bottom of the phase space, indicating higher likelihood of formation compared to

the binary oxides of Fe and Co having relatively larger absolute values of ΔH_f (over 1.5 eV/atom). Going forward to the ternary and quaternary phases, it is also crucial to consider the phases without Co. In the sub-space of the CaO-SiO₂-Al₂O₃-MgO (CSAM) system, a large number of phases are possible, which evidently reside around the energetic bottom of the compositional space. To demonstrate this, some well-known phases (e.g., CaMgSi₂O₆ (1), Ca₂SiO₄ (2), etc.) are shown in Fig. 8 and highlighted in the inset. Upon inclusion of Fe, further possible phases appear in the space such as Fe₂SiO₄ (3) and MgFe₂O₄ (4), naturally residing between the binary oxides of Fe and Mg/ Si. In fact, in industrial fayalite slags, these diopside and fayalite phases are known to form within the amorphous matrix [5]. After adding the recovery element Co to the pool, the phases within the slag composition with lowest



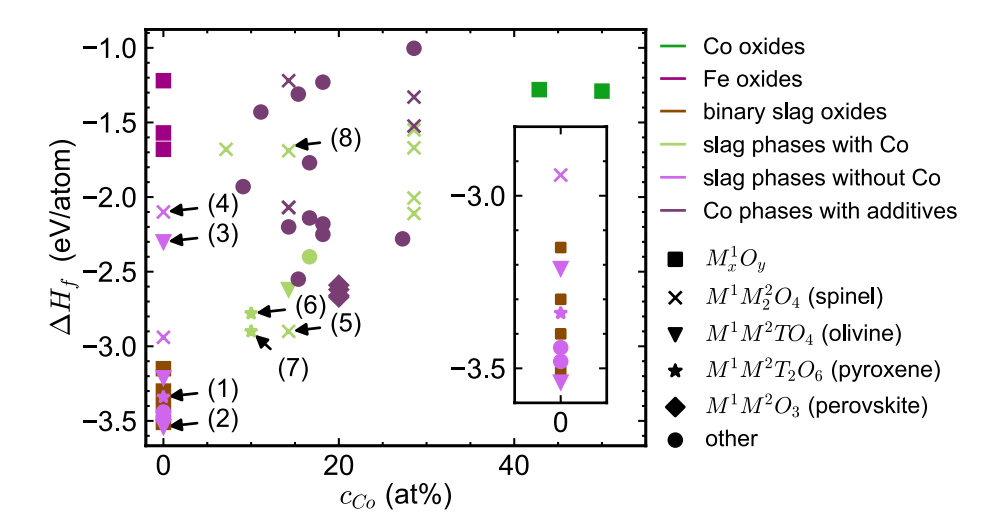


Fig. 8 Formation energy values in the compositional space of the considered slag system obtained through DFT calculations. The ΔH_f as a function of the atomic Co content in the corresponding phases is considered to identify potential Co-containing EnAM phases and respective additives. Numbered data points correspond to the dis-

cussed crystalline phases. The structure formulas are generalized according to the cations present in the respective crystallographic groups with M being a metal cation and T being the Si^{+4} cation as considered in this work

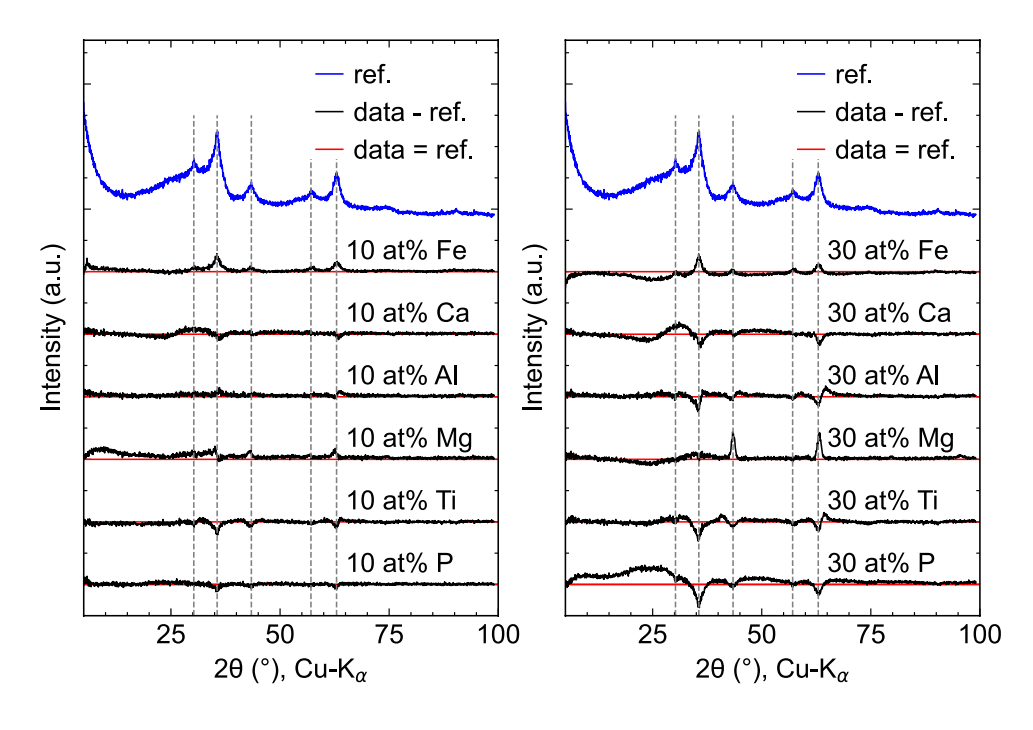
 ΔH_f are identified as CoAl_2O_4 (5), $\text{MgCoSi}_2\text{O}_6$ (6) and CaCoSiO_6 (7), whereas CoFe_2O_4 (8) appears relatively high in the compositional space.

In search for external additives that can potentially promote formation of EnAM, the Co-containing phases having ΔH_f below -2.0 eV/atom and at least 18 at.% of Co are considered. It was found that among the pool, ACoO₃ (A=Ti, Y, Sm, Ho, La) has ΔH_f in the range of -2.6 to -2.65 eV/atom with 20 at.% Co. Therefore, Ti was considered as a potential additive in subsequent experiments to

investigate its effect on slag crystallization. Further, Fe, Mg, Ca, Al, and P are considered as additives through increasing their content in the model slag during the FSP synthesis. Given the fast cooling rates of FSP synthesis, the objective at this point is to investigate whether the phases with lowest ΔH_f actually form in the process to gain knowledge about the crystallization behavior of the chemically diverse slag system.

The effect of additives on the slag crystallization is assessed by means of X-ray diffraction (XRD)

Fig. 9 Effect of additives on assprayed slag crystallinity. The normalized XRD data of the reference sample (blue line) are subtracted from the sample data resulting in the shown XRD difference plots (black lines). The elemental atomic fractions indicate the nominal additive amount in the FSP precursor (cf. Figure 2)





measurements, as shown in Fig. 9. All data are normalized with respect to their respective diffraction intensity maxima prior to analysis to account for, e.g., aging effects of the diffractometer X-ray source on the results. Here, sample 1 without any nominal elemental addition in the FSP precursor is taken as a reference sample (cf. Figure 3a) and subsequently subtracted from the sample data to highlight the effect of the respective additive. Positive values of the XRD difference plots indicate an intensity increase for the specific 2θ angle and vice versa.

The reference diffractograms reveal a crystalline-amorphous structure in virtue of distinct, yet broad intensity peaks and the characteristic convex halo between 20° and 40° . The marked intensity peaks exclusively indicate the presence of a cubic spinel-structure $(Fd\overline{3}m)$, with peaks solely belonging to other crystal groups absent. Consequently, the formation of spinels is preferred over olivines or pyroxenes, despite the significantly lower ΔH_f of the latter, which indicates that the crystallization of the system is influenced by the FSP process kinetics. Due to the chemical complexity of the system, it is likely that this crystalline structure comprises more than one phase. However, owing to extensive peak broadening caused by nanosized crystals, precise identification of the phase composition is limited by examining XRD alone.

Increasing the content of a slag constituent or adding a new element to the system leads to two principal observations. Firstly, increasing an elemental content may suppress crystallization of the slag nanoparticles during synthesis. This effect is caused by Ca and P, where in the latter case, the sample is fully amorphous at a nominal P concentration of 30 at.% in the precursor solution. In the corresponding difference plots, the measured intensities notably decrease only in correspondence of the peaks in the reference measurement, indicating an amorphization with or without the crystallization of further phases. Both observations are in line with experimentally reported findings. From a technological point of view, crystallization of an EnAM using phosphorus as an additive would be beneficial because it is

considered a major contaminant in metal production and, hence, it is confined to the slag phase during dephosphorization [56]. However, given its effect of suppressing crystallization, P can be neglected as future slag additive, whereas it is in fact used as an additive in glass production [57]. Further, it was found that increasing the amount of Ca as an additive promotes the formation of a glassy phase in the FeO_x-SiO₂-CaO model slag system. However, having the slag produced under reducing conditions, the main crystalline phase is fayalite (Fe₂SiO₄) which, upon adding CaO, is co-existing with hedenbergite CaFeSi₂O₆. [8] Both silicates have been found in fayalitic slag microstructures along with other complex oxides such as spinels (e.g., MgAl₂O₄, FeAl₂O₄), olivines (e.g., Mg₂SiO₄, CaFeSiO₄), and pyroxenes (e.g., FeCaSi₂O₆) [5]. Hence, the defined compositional space provides an accurate summary of crystalline phases observed in real slag systems.

Secondly, an additive may promote the crystallization of a different or new phase compared to the reference sample. The investigated additives Fe, Al, Ti, and Mg reveal three different influences. Upon adding Fe, the peak diffraction intensities increase at the locations of the reference measurement and overall crystallinity is improved. Adding Al and Ti leads to peak shifts towards greater diffractions angles. Adding Mg results in two distinct intensity rises around 20 angles of 43.40° and 63.15°. These observations can be put into a broader perspective by looking at the elemental mappings of a primary particle shown in Fig. 10.

The structure analysis in Fig. 9 showed that the crystallization of isomorphous cubic spinel phases is predominant. Considering the extensive peak broadening, the identification of phases represents a challenging task without knowledge on which elements actually contribute to crystallization. Therefore, the reference sample is analyzed with EDX in HRTEM measurements (Fig. 10). The elemental mappings displaying the individual net count intensities reveal a heterogeneous distribution of the slag elements within a primary nanoparticle. The spatial distribution of Fe strongly

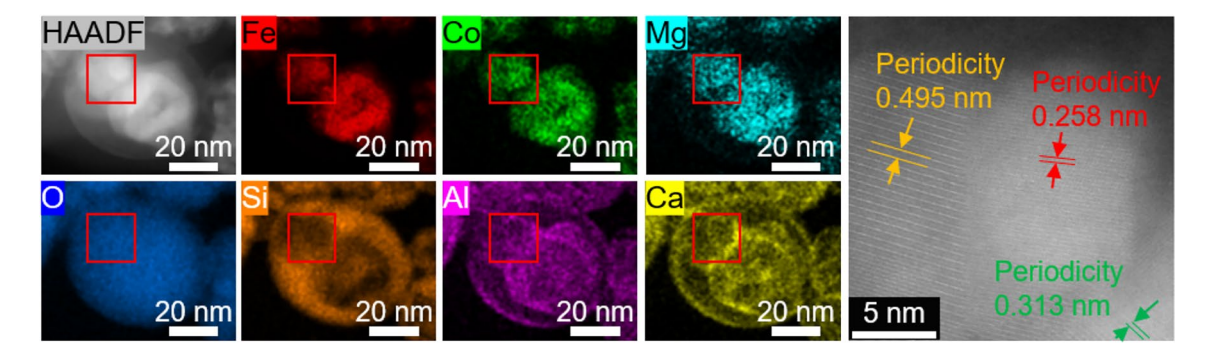


Fig. 10 HAADF image and EDX elemental mappings revealing a heterogenous element distribution within the primary nanoparticles and nanocrystallinity



correlates with Co and Mg, whereas all three elements are embedded in a matrix of Si. Al and Ca seem to be enriched at the interface between the Si-rich and the Fe–Co–Mg-rich regions, and O is distributed homogenously across the examined primary particle. Notably, the Fe–Co–Mg-rich region is characterized by nano-crystallinity, as shown in the right STEM image. Further, no crystal fringes are observed in the Si-rich region, indicating the presence of an amorphous matrix. This matches with the XRD data which indicate both crystalline and amorphous material fractions. It is, therefore, concluded that the observed peaks in the previously discussed XRD measurements correspond to one or more spinel phases containing at least the elements Fe, Co, Mg, and O.

As discussed initially, slag nanoparticles were produced through the gas-to-particle route. For this particle formation mechanism, phase segregation has been observed in FSP synthesis when spraying Si and Fe precursor mixtures, which resulted in precipitated Fe₂O₃ within a SiO₂ shell [58], similar to the elemental distribution shown in Fig. 10. The particle configuration arises due to limited phase miscibility or solid-state reactions, creating a diffusion barrier at the phase interface [18]. In case of the investigated slag sample, the encapsulated crystalline phase consists of Fe, Co, and Mg, which indicates good miscibility of these elements during particle formation. According to Goldschmidt's rule, formation of solid solutions between the spinels Mg ferrite and Co ferrite is likely to occur, as investigated in [59]. Elsewhere, the effect of adding FeO_x to the CSAM system was investigated [60]. Here, FeO_x acted as a nucleant for crystallization of the pyroxene diopside (CaMgSi₂O₆). The enrichment of Ca and Al at the encapsulation layer may indicate the formation of an oxide layer as proposed in [18]. Reconsidering the above-mentioned additive effects on slag crystallinity, the observed peak shifts (Al, Ti) may be attributed to improved miscibility with the segregated crystalline core phase when respective element contents are increased. The rise of peak intensities when adding Fe and Mg underlines that these elements crystallize already in the reference sample as the diffraction peak locations still coincidence with the reference measurement.

The experimental findings, together with the defined compositional space (cf. Figure 8), provide a comprehensive insight in the crystallization of the investigated slag systems. Rather than crystallizing as the $CoAl_2O_4$ phase, Al mingles in the sub-space of the CSAM because the competing phases possess even lower ΔH_f than the Co aluminate. Instead, Co ferrite is forming in a solid solution with Mg ferrite. However, this picture might alter to some extent with different synthesis conditions, e.g., cooling rates, as they greatly impact slag crystallization [5].

The formation of spinel phases is thermodynamically favorable and readily obtained in the FSP process. To support the findings from the XRD and EDX/STEM analyses, a new slag sample with a significantly decreased Si content is synthesized to minimize the amount of amorphous phases (cf. Figure 3d). Figure 11 compares the XRD pattern of this Si-depleted slag with the patterns of the single phases CoFe₂O₄ and MgFe₂O₄. It is apparent that the diffractograms of either pure phases match the slag sample data reasonably well in the examined 2θ range. As assumed earlier, this observation indicates that more than one isomorphous spinel phase is crystallizing and potentially forming a solid solution. Secondly, decreasing the silicon content leaves the crystallization behavior of the system unaffected and solely decreases the content of the amorphous matrix around the crystalline nanoparticles. Considering the findings above, it is concluded that the Fe-Co-Mg-O system is a potential candidate for an EnAM aiming at Co recovery from fayalitic slags, especially the spinel phase CoFe₂O₄.

Conclusion

An approach to investigate the crystallization of a fayalitic model slag within the scope of Co recycling through EnAMs was introduced. The approach consists of slag synthesis and characterization experiments supported by ab initio DFT calculations of ΔH_f values. It was demonstrated that model slags can be produced with freely engineerable compositions with FSP synthesis. Through appropriate precursor design, the gas-to-particle formation route ensures chemically homogeneous metal oxide nanoparticle aggregates of up to eight different elements. Calculated ΔH_f values are used to predict the thermodynamic stabilities of phases that can be gas phase synthesized as validated by XRD measurements and the Rietveld refinements. From a comprehensive

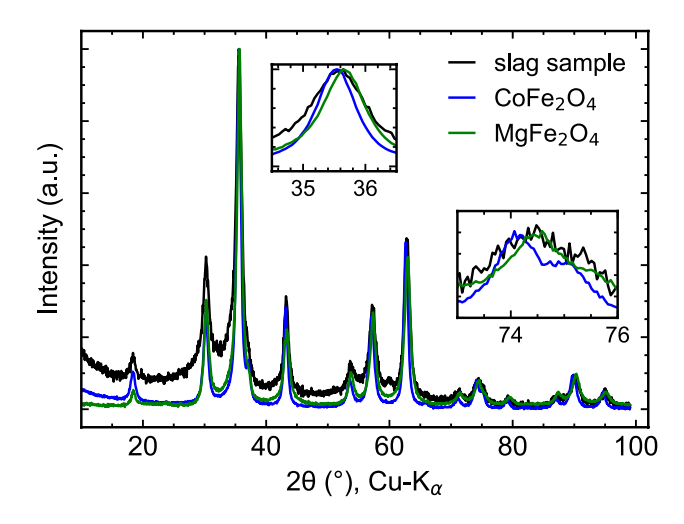


Fig. 11 XRD data of as-sprayed slag with decreased Si content. The comparison with the single-phase data indicates the crystallization of isomorphous CoFe_2O_4 and MgFe_2O_4



theoretical exploration of the compositional space of the slag system and subsequent slag characterization experiments, it is concluded that Co forms a solid-solution spinel in the Fe-Mg-Co-O system, owing to the elemental miscibility under the out-of-equilibrium conditions during FSP synthesis. Based on the experimental and theoretical findings, a reasonable prerequisite for Co recycling through engineerable crystallization seems to be a minimum of Fe content in the slag. Future investigations will look into the melting and recrystallization of the model slags under controlled cooling rates in order to confirm the EnAM character of the hereidentified (Co,Mg)Fe₂O₄. Despite being synthesized in the gas phase, melting and thermal processing will ensure the comparability of the physical and mineralogical properties of the model slags with real metallurgical systems. The work will include the quantification of smelting and cooling conditions to obtain EnAM crystals with sufficient sizes and Co loading, thus, making them suitable for downstream liberation from the slag matrix.

Acknowledgements We would like to thank the German Research Foundation DFG for funding this work within the priority program PP2315 "Engineered Artificial Minerals" under grants MA 3333/27-1 and CO 1043/26-1. We further thank Petra Witte for performing the SEM/EDX measurements and Dr. Tim Grieb for performing HRTEM/EDX measurements.

Author Contributions MV: methodology, formal analysis, investigation, data curation, writing—original draft, writing—review and editing, visualization, KP: methodology, formal analysis, software, investigation, writing—original draft, LCC: conceptualization, writing—review and editing, supervision, resources, funding acquisition, LM: conceptualization, writing—review and editing, supervision, resources, funding acquisition.

Funding Open Access funding enabled and organized by Projekt DEAL.

Data Availability Data will be made available on request.

Declarations

Competing interests The authors declare that they have no known competing financial interests or personal relationships that could have appeared to influence the work reported in this paper.

Open Access This article is licensed under a Creative Commons Attribution 4.0 International License, which permits use, sharing, adaptation, distribution and reproduction in any medium or format, as long as you give appropriate credit to the original author(s) and the source, provide a link to the Creative Commons licence, and indicate if changes were made. The images or other third party material in this article are included in the article's Creative Commons licence, unless indicated otherwise in a credit line to the material. If material is not included in the article's Creative Commons licence and your intended use is not permitted by statutory regulation or exceeds the permitted use, you will need to obtain permission directly from the copyright holder. To view a copy of this licence, visit http://creativecommons.org/licenses/by/4.0/.

References

- Alves Dias P, Blagoeva D, Pavel C, Arvanitidis N (2018) Cobalt: demand-supply balances in the transition to electric mobility, vol EUR 29381 EN. Publications Office of the European Union, Luxembourg
- Phiri TC, Singh P, Nikoloski AN (2022) The potential for copper slag waste as a resource for a circular economy: a review—Part I. Miner Eng. https://doi.org/10.1016/j.mineng.2022.107474
- Karimi N, Vaghar R, Mohammadi MRT, Hashemi SA (2013) Recovery of copper from the slag of Khatoonabad flash smelting furnace by flotation method. J Inst Eng (India) 94(1):43–50. https://doi.org/10.1007/s40033-013-0015-3
- Parada F, Sanchez M, Ulloa A, Carrasco JC, Palacios J, Reghezza A (2013) Recovery of molybdenum from roasted copper slags. Miner Process Extr Metall 119(3):171–174. https://doi.org/10. 1179/037195510x12772935654701
- Phiri TC, Singh P, Nikoloski AN (2021) The potential for copper slag waste as a resource for a circular economy: a review—Part II. Miner Eng. https://doi.org/10.1016/j.mineng.2021.107150
- Shi C, Meyer C, Behnood A (2008) Utilization of copper slag in cement and concrete. Resour Conserv Recycl 52(10):1115–1120. https://doi.org/10.1016/j.resconrec.2008.06.008
- Yang Z, Rui-lin M, Wang-dong N, Hui W (2010) Selective leaching of base metals from copper smelter slag. Hydrometallurgy 103(1-4):25-29. https://doi.org/10.1016/j.hydromet.2010.02.009
- Simon S, Gluth GJG, Peys A, Onisei S, Banerjee D, Pontikes Y (2017) The fate of iron during the alkali-activation of synthetic (CaO-)FeOx-SiO2 slags: An Fe K-edge XANES study. J Am Ceram Soc 101(5):2107–2118. https://doi.org/10.1111/jace.15354
- Shen Y, Chong J, Huang Z, Tian J, Zhang W, Tang X et al (2019) Viscosity and structure of a CaO-SiO(2)-FeO-MgO system during a modified process from nickel slag by CaO. Materials (Basel). https://doi.org/10.3390/ma12162562
- Mihailova I, Mehandjiev D (2010) Characterization of fayalite from copper slags. J Univ Chem Technol Metall 45(3):317–26
- Rao MD, Singh KK, Morrison CA, Love JB (2020) Challenges and opportunities in the recovery of gold from electronic waste. RSC Adv 10(8):4300–4309. https://doi.org/10.1039/c9ra07607g
- Doose S, Mayer JK, Michalowski P, Kwade A (2021) Challenges in ecofriendly battery recycling and closed material cycles: a perspective on future lithium battery generations. Metals. https://doi. org/10.3390/met11020291
- Windisch-Kern S, Holzer A, Ponak C, Raupenstrauch H (2021) Pyrometallurgical lithium-ion-battery recycling: approach to limiting lithium slagging with the indured reactor concept. Processes. https://doi.org/10.3390/pr9010084
- Buchmann M, Borowski N, Leißner T, Heinig T, Reuter MA, Friedrich B et al (2020) Evaluation of recyclability of a WEEE slag by means of integrative X-ray computer tomography and SEM-based image analysis. Minerals. https://doi.org/10.3390/min10040309
- Schnickmann A, Hampel S, Schirmer T, Fittschen UEA (2023)
 Formation of lithium-manganates in a complex slag system consisting of Li2O-MgO-Al2O3-SiO2-CaO-MnO—a first survey.
 Metals. https://doi.org/10.3390/met13122006
- Zgheib A, Fischer MH, Namyslo JC, Fittschen UEA, Wollmann A, Weber AP et al (2024) Photo-switchable collectors for the flotation of lithium aluminate for the recycling of the critical raw material lithium. ChemSusChem. https://doi.org/10.1002/cssc. 202301900
- Schirmer T, Hiller J, Weiss J, Munchen D, Lucas H, Fittschen UEA et al (2024) Behavior of tantalum in a Fe-dominated synthetic fayalitic slag system—phase analysis and incorporation. Minerals. https://doi.org/10.3390/min14030262



- Teoh WY, Amal R, M\u00e4dler L (2010) Flame spray pyrolysis: an enabling technology for nanoparticles design and fabrication. Nanoscale 2(8):1324

 –1347. https://doi.org/10.1039/c0nr00017e
- FIZ Karlsruhe—Leibniz Institute for Information Infrastructure Inorganic Crystal Structure Database—ICSD. http://www.fiz-karlsruhe.com/icsd.html. Accessed 10 Jan 2024
- Hohenberg P, Kohn W (1964) Inhomogeneous electron gas. Phys Rev 136(3B):B864–B871. https://doi.org/10.1103/PhysRev.136. B864
- Kohn W, Sham LJ (1965) Self-consistent equations including exchange and correlation effects. Phys Rev 140(4A):A1133– A1138. https://doi.org/10.1103/PhysRev.140.A1133
- Giannozzi P, Baroni S, Bonini N, Calandra M, Car R, Cavazzoni C et al (2009) QUANTUM ESPRESSO: a modular and open-source software project for quantum simulations of materials. J Phys Condens Matter 21(39):395502. https://doi.org/10.1088/0953-8984/21/39/395502
- Giannozzi P, Andreussi O, Brumme T, Bunau O, Buongiorno Nardelli M, Calandra M et al (2017) Advanced capabilities for materials modelling with QUANTUM ESPRESSO. J Phys Condens Matter 29(46):465901. https://doi.org/10.1088/1361-648X/ aa8f79
- Prandini G, Marrazzo A, Castelli IE, Mounet N, Marzari N (2018) Precision and efficiency in solid-state pseudopotential calculations. npj Comput Mater. https://doi.org/10.1038/s41524-018-0127-2
- A Standard Solid State Pseudopotentials (SSSP) library optimized for precision and efficiency (2023). Materials Cloud Archive. https://archive.materialscloud.org/record/2023.65. Accessed 24 Sept 2023
- Anisimov VI, Zaanen J, Andersen OK (1991) Band theory and Mott insulators: Hubbard U instead of Stoner I. Phys Rev B 44(3):943–954. https://doi.org/10.1103/physrevb.44.943
- Cococcioni M, de Gironcoli S (2005) Linear response approach to the calculation of the effective interaction parameters in theLDA+Umethod. Phys Rev. https://doi.org/10.1103/PhysRevB. 71.035105
- Kulik HJ, Cococcioni M, Scherlis DA, Marzari N (2006) Density functional theory in transition-metal chemistry: a self-consistent Hubbard U approach. Phys Rev Lett 97(10):103001. https://doi. org/10.1103/PhysRevLett.97.103001
- Timrov I, Marzari N, Cococcioni M (2022) HP—a code for the calculation of Hubbard parameters using density-functional perturbation theory. Comput Phys Commun. https://doi.org/10. 1016/j.cpc.2022.108455
- Mutter D, Urban DF, Elsasser C (2020) Determination of formation energies and phase diagrams of transition metal oxides with DFT+U. Materials (Basel). https://doi.org/10.3390/ma13194303
- 31. Jain A, Hautier G, Ong SP, Moore CJ, Fischer CC, Persson KA et al (2011) Formation enthalpies by mixing GGA and GGA+Ucalculations. Phys Rev B. https://doi.org/10.1103/PhysRevB.84.045115
- Wang L, Maxisch T, Ceder G (2006) Oxidation energies of transition metal oxides within theGGA+Uframework. Phys Rev B. https://doi.org/10.1103/PhysRevB.73.195107
- Pokhrel S, Stahl J, Groeneveld JD, Schowalter M, Rosenauer A, Birkenstock J et al (2023) Flame aerosol synthesis of metal sulfides at high temperature in oxygen-lean atmosphere. Adv Mater 35(28):e2211104. https://doi.org/10.1002/adma.202211104
- Meierhofer F, Mädler L, Fritsching U (2019) Nanoparticle evolution in flame spray pyrolysis—Process design via experimental and computational analysis. AIChE J. https://doi.org/10.1002/aic. 16885
- 35. Mädler L, Kammler HK, Mueller R, Pratsinis SE (2002) Controlled synthesis of nanostructured particles by flame spray

- pyrolysis. J Aerosol Sci 33(2):369–389. https://doi.org/10.1016/ S0021-8502(01)00159-8
- Balakrishnan A, Groeneveld JD, Pokhrel S, Mädler L (2021) Metal sulfide nanoparticles: precursor chemistry. Chemistry 27(21):6390–6406. https://doi.org/10.1002/chem.202004952
- Jossen R, Pratsinis SE, Stark WJ, M\u00e4dler L (2005) Criteria for flame-spray synthesis of hollow, shell-like, or inhomogeneous oxides. J Am Ceram Soc 88(6):1388–1393. https://doi.org/10. 1111/j.1551-2916.2005.00249.x
- Venkatesan S, Mitzel J, Wegner K, Costa R, Gazdzicki P, Friedrich KA (2022) Nanomaterials and films for polymer electrolyte membrane fuel cells and solid oxide cells by flame spray pyrolysis. Renew Sustain Energy Rev. https://doi.org/10.1016/j.rser.2022.112080
- Strobel R, Pratsinis SE (2011) Effect of solvent composition on oxide morphology during flame spray pyrolysis of metal nitrates. Phys Chem Chem Phys 13(20):9246–9252. https://doi.org/10. 1039/c0cp01416h
- Stodt MFB, Groeneveld JD, Mädler L, Kiefer J, Fritsching U (2022) Microexplosions of multicomponent drops in spray flames. Combus Flame. https://doi.org/10.1016/j.combustflame.2022. 112043
- Rosebrock CD, Wriedt T, M\u00e4dler L, Wegner K (2015) The role of microexplosions in flame spray synthesis for homogeneous nanopowders from low-cost metal precursors. AIChE J 62(2):381–391. https://doi.org/10.1002/aic.15056
- Li H, Rosebrock CD, Wu Y, Wriedt T, M\u00e4dler L (2019) Single droplet combustion of precursor/solvent solutions for nanoparticle production: optical diagnostics on single isolated burning droplets with micro-explosions. Proc Combust Inst 37(1):1203–1211. https://doi.org/10.1016/j.proci.2018.06.133
- 43. Meierhofer F, Li H, Gockeln M, Kun R, Grieb T, Rosenauer A et al (2017) Screening precursor-solvent combinations for Li(4) Ti(5)O(12) energy storage material using flame spray pyrolysis. ACS Appl Mater Interfaces 9(43):37760–37777. https://doi.org/10.1021/acsami.7b11435
- Rosebrock CD, Riefler N, Wriedt T, M\u00e4dler L, Tse SD (2013) Disruptive burning of precursor/solvent droplets in flame-spray synthesis of nanoparticles. AIChE J 59(12):4553

 4566. https://doi.org/10.1002/aic.14234
- Chase MW Jr (1998) NIST-JANAF thermochemical tables. J Phys Chem Ref Data 1-1951
- Bartel CJ, Trewartha A, Wang Q, Dunn A, Jain A, Ceder G (2020)
 A critical examination of compound stability predictions from machine-learned formation energies. Npj Comput Mater. https://doi.org/10.1038/s41524-020-00362-y
- Peterson GGC, Brgoch J (2021) Materials discovery through machine learning formation energy. J Phys Energy 3(2):022002. https://doi.org/10.1088/2515-7655/abe425
- 48. Meredig B, Agrawal A, Kirklin S, Saal JE, Doak JW, Thompson A et al (2014) Combinatorial screening for new materials in unconstrained composition space with machine learning. Phys Rev B 89(9):094104. https://doi.org/10.1103/PhysRevB.89.094104
- Sun W, Dacek ST, Ping Ong S, Hautier G, Jain A, Richards WD et al (2016) The thermodynamic scale of inorganic crystalline metastability. Sci Adv 2(11):e1600225. https://doi.org/10.1126/sciadv.1600225
- Lejaeghere K, Van Speybroeck V, Van Oost G, Cottenier S (2013) Error estimates for solid-state density-functional theory predictions: an overview by means of the ground-state elemental crystals. Crit Rev Solid State Mater Sci 39(1):1–24. https://doi.org/10.1080/10408436.2013.772503
- Shannon RD (1976) Revised effective ionic radii and systematic studies of interatomic distances in halides and chalcogenides. Acta Crystallogr A 32:751–767. https://doi.org/10.1107/S056773947 6001551



- 52. Horlyck J, Pokhrel S, Lovell E, Bedford NM, M\u00e4dler L, Amal R et al (2019) Unifying double flame spray pyrolysis with lanthanum doping to restrict cobalt–aluminate formation in Co/Al2O3 catalysts for the dry reforming of methane. Catal Sci Technol 9(18):4970–4980. https://doi.org/10.1039/c9cy01293a
- Piriyasurawong K, Piticharoenphun S, Mekasuwandumrong O (2018) One-step FSP synthesis of nanocrystalline Fe/Al2O3 and Fe-Ce/Al2O3 catalyst for CO2 hydrogenation reaction. Mater Sci Forum 916:134–138. https://doi.org/10.4028/www.scientific.net/ MSF.916.134
- 54. Li Y, Hu Y, Huo J, Jiang H, Li C, Huang G (2012) Stable core shell Co3Fe7–CoFe2O4 nanoparticles synthesized via flame spray pyrolysis approach. Ind Eng Chem Res 51(34):11157–11162. https://doi.org/10.1021/ie3010644
- 55. Sameer K, Azurdia JA, Laine RM (2010) Synthesis of (MgO) x(Fe2O3)1-x nanoparticles via liquid feed flame spray pyrolysis. A non-stoichiometric spinel phase outside the normal phase diagram. J Ceram Process Res 11(5):517–522
- Li F, Li X, Zhang Y, Gao M (2019) Phosphate capacities of CaO-FeO-SiO2-Al2O3/Na2O/TiO2 slags. High Temp Mater

- Process (London) 38(2019):50-59. https://doi.org/10.1515/htmp-2017-0151
- Velikanova EY, Gorashchenko NG (2011) Effect of phosphorous oxide additives on the color and production conditions of Bi₂O₃-SiO₂-P₂O₅ glass. Glass Ceram 68:209–210
- Hirt AM, Sotiriou GA, Kidambi PR, Teleki A (2014) Effect of size, composition, and morphology on magnetic performance: first-order reversal curves evaluation of iron oxide nanoparticles. J Appl Phys. https://doi.org/10.1063/1.4863543
- Dojcinovic MP, Vasiljevic ZZ, Pavlovic VP, Barisic D, Pajic D, Tadic NB et al (2021) Mixed Mg–Co spinel ferrites: structure, morphology, magnetic and photocatalytic properties. J Alloys Compds. https://doi.org/10.1016/j.jallcom.2020.157429
- Shi Y, Han X-X, Li B-W, Chen Y-X, Zhang M-X (2020) Modification of glass network and crystallization of CaO

 –Al2O3

 –MgO

 –SiO2 based glass ceramics with addition of iron oxide. Ceram Int 46(7):9207

 –9217. https://doi.org/10.1016/j.ceramint.2019.12.173

Publisher's Note Springer Nature remains neutral with regard to jurisdictional claims in published maps and institutional affiliations.

Authors and Affiliations

Manuel Vollbrecht¹ · Krishnanjan Pramanik^{1,3} · Lucio Colombi Ciacchi^{1,3} · Lutz Mädler^{1,2}

- ☐ Lutz Mädler lmaedler@iwt.uni-bremen.de
- University of Bremen, Faculty of Production Engineering and MAPEX Center for Materials and Processes, Bibliothekstr. 1, 28359 Bremen, Germany
- ² Leibniz Institute for Materials Engineering IWT, Badgasteiner Str. 3, 28359 Bremen, Germany
- ³ Hybrid Materials Interfaces Group, Bremen Center for Computational Materials Science, University of Bremen, Am Fallturm 1, 28359 Bremen, Germany

